Experimental and numerical thermal analysis for direct microwave heating of silicon carbide

Inès Ghorbel, Patrick Ganster, Nicolas Moulin, Christophe Meunier, Julien Bruchon

Received <day> <Month>, <year>; | Revised <day> <Month>, <year>; | Accepted <day> <Month>, <year>

DOI: xxx/xxxx

ARTICLE TYPE

Experimental and numerical thermal analysis for direct microwave heating of Silicon Carbide

Inès Ghorbel | Patrick Ganster | Nicolas Moulin* | Christophe Meunier | Julien Bruchon

[1]Mines Saint-Étienne, Univ. Lyon, CNRS, UMR 5307 LGF, Centre SMS, F - 42023 Saint-Étienne, France

Correspondence
*Nicolas Moulin, Mines Saint-Étienne, 158 cours Fauriel, 42023 Saint-Étienne cedex 02, France. Email: nicolas.moulin@emse.fr

Abstract

A comparison between experiment and numerical simulation of microwave heating of a parallelepipedic silicon carbide (SiC) sample is presented. Using a 2.45 GHz single-mode cavity, the evolution of the surface temperature is first experimentally studied for different orientations of the sample. A finite element analysis of this electromagnetic - thermal coupled problem is then conducted with the COMSOL Multiphysics® software. Despite the different approximations of our model, a good agreement between experimental and numerical results is found, confirming that the heating of SiC depends only on the electric field. The effect of sample orientations and the cavity length on heating is also highlighted and analyzed.

KEYWORDS:
microwave heating; numerical simulation; silicon carbide (SiC)

HIGHLIGHTS

- Numerical and experimental study of microwave heating of a parallelepipedic silicon carbide sample.
- Investigation of the effect of sample orientation in the electric field.
- Emissivity measurement silicon carbide (SiC).
- Impact of sample dimensions and cavity length on the microwave heating.

NOMENCLATURE

Electromagnetic symbols

- **E** electric field (V.m^{-1})
- **H** magnetic field (A.m^{-1})
- **D** electric displacement field (C.m^2)
- **P** dielectric polarization field (C.m^2)
- ε_r complex relative permittivity (F.m^{-1})
- $\varepsilon_r^{''}$ relative permittivity imaginary part (F.m^{-1})
- ε_0 vacuum permittivity ($8.85418782 \times 10^{-12}$ F.m^{-1})
- μ_r complex relative permeability (H.m^{-1})
- $\mu_r^{''}$ relative permeability imaginary part (H.m^{-1})
- μ_0 vacuum permeability ($4\pi \times 10^{-7}$ H.m^{-1})
- σ_e electric conductivity (S.m^{-1})
- ω angular frequency (rad.s^{-1})
- j the complex number
- P_{in} incident power (W)
- P_r reflected power (W)

Thermal symbols

- $\overline{\rho}$ density (kg.m^{-3})
- C_p specific heat (J.kg^{-1}.K^{-1})
- κ thermal conductivity (W.m^{-1}.K^{-1})
- Φ heat flux (W.m^{-2})
- Φ_r surface to ambient radiative heat flux (W.m^{-2})

- Φ_c convective heat flux (W.m^{-2})
- σ_B Stefan-Boltzmann constant (5.670367×10^{-8} W.m^{-2}.K^{-4})
- ϵ emissivity
- Q_{EM} heat source (W.m^{-3})
- h heat transfer coefficient (5 W.m^{-2}.K^{-1})
- T temperature (K)
- T_{amb} ambient temperature (K)

1 | INTRODUCTION

The sintering process by microwave heating has been studied over the last decades, both in the context of basic research [1] and industrial applications, for various materials such as metals [2–4], ceramics [5–9] and composites [10, 11]. Due to the penetration of the electromagnetic wave into the material, this process offers volumetric heating, selective heating, low energy consumption and short processing time. This work focuses on ceramic materials, which have no or low magnetic loss. In this case, the contribution of the magnetic field to microwave heating is negligible [12–14]. Hence, the heating is only due to the electric field, and is governed by the dielectric loss. In fact, only materials with a high dielectric loss at room temperature (silicon carbide, zinc oxide, etc) can be efficiently heated in direct configuration, *i.e* without using a susceptor [15]. For materials with low dielectric loss (such as alumina), a hybrid configuration using a susceptor, usually in Silicon Carbide (SiC), should be used to initiate microwave heating [7–9].

Despite all benefits of microwave heating, the process is difficult to control. Indeed, conventional temperature measuring devices, such as thermocouples, can not be used as it interacts with microwaves. For this reason, non-contact devices such as infrared pyrometers and/or thermal cameras are more suitable for monitoring and controlling the process and they must in any case be calibrated [9, 16]. In the case of single mode configuration, another difficulty comes from the sample position which has to be in a maximum of electric field for an efficient heating. In addition, the sample tends to disturb the electromagnetic field during heating due to the evolution of its dielectric properties with the temperature. This implies that the stationary wave remains no longer stationary and the position of the short-circuit piston has to be continuously changed to control the heating.

Understanding microwave sintering requires a multidisciplinary perspective, combining electromagnetic, thermal and mechanical approaches. Indeed, the propagation of an electromagnetic wave in a material generates heat dissipation, leading to

temperature heterogeneities, which is turn active mass transport mechanisms resulting in densification of the material[17]. Moreover, the thermo-physical parameters involved in the description of these phenomena (specific heat C_p, thermal conductivity κ and complex relative permittivity ε_r), depend strongly on both temperature and density. To tackle this complexity, the numerical simulations are often associated with experiments to evaluate temperature fields[2, 6–8, 18–23] in cylindrical or hexagonal samples.

The purpose and the originality of this work is to study experimentally and numerically the direct microwave heating of a parallelepipedic SiC sample with different orientations in a single-mode cavity excited at 2.45 GHz.

The rest of this paper consists of four parts. First, the theory of microwave heating is presented. Next, the experimental procedure used to measure the surface temperature with a pyrometer is described. The third section is devoted to numerical simulations performed with COMSOL Multiphysics® software[24]. The experimental and numerical results are then discussed and confronted before to conclude.

2 | MICROWAVE HEATING THEORY

2.1 | Equations of electric and temperature fields

Let us consider the single-mode microwave cavity in which a sample of SiC is placed on an insulating support having a very low dielectric loss. The figure 1 presents a 2D schematic of this cavity which corresponds to a waveguide delimited by an iris and a short-circuit piston. Cavity is denoted by the domain $\Omega_{waveguide}$. Inside the cavity, the sample, corresponding to the domain Ω_{sample}, is placed on an insulating support which corresponds to the domain $\Omega_{support}$.

The mathematical description of heating in a single mode cavity of this SiC sample, is based on two coupled equations. One is dedicated to calculate the electric field and its evolution in the cavity and the materials inside (sample and insulating support), the other is dedicated to calculate the temperature field.

The equation determining the electric field is obtained by a combination of Maxwell's equations[25, 26]:

$$\nabla \times (\mu_r^{-1} \nabla \times \mathbf{E_r}) = k_0^2 \left(\varepsilon_r - \frac{j\sigma_e}{\omega \varepsilon_0} \right) \mathbf{E_r} \tag{1}$$

where μ_r is the complex relative permeability, ε_r the complex relative permittivity, σ_e the electric conductivity, ω the microwave angular frequency, ε_0 the vacuum permittivity, and $k_0^2 = \omega^2 \mu_0 \varepsilon_0$ the vacuum wave number, with μ_0 the vacuum permeability. In Equation 1, the term $\sigma_e/\omega\varepsilon_0$ corresponds to the electrical conductivity component in the permittivity imaginary part. Moreover, in this expression, the electric field $\mathbf{E}$ has been written in the form $\mathbf{E} = \mathbf{E_r} \exp(j\omega t)$ where t is the time variable and j the complex number such as j^2=−1. Equation (1) has to be solved in the whole domain $\Omega = \Omega_{\text{waveguide}} \cup \Omega_{\text{sample}} \cup \Omega_{\text{support}}$ (Figure 1) in which the material parameters are respectively those of air, SiC and insulating material.

The thermal problem, defined only in the heated subdomain $\Omega_{\text{sample}} \cup \Omega_{\text{support}}$, writes:

$$\overline{\rho} C_p \frac{dT}{dt} + \nabla \cdot (-\kappa \nabla T) = Q_{EM} \tag{2}$$

where T is the temperature field, $\overline{\rho}$ the density, C_p the specific heat, and κ the thermal conductivity. The term Q_{EM} corresponds to the heat source expressing the coupling between the electromagnetic field and the thermal problem:

$$Q_{EM} = \frac{1}{2}[\omega \varepsilon_0 \varepsilon_r'' \mathbf{E}^2 + \omega \mu_0 \mu_r'' \mathbf{H}^2] \tag{3}$$

where ε_r'' is the imaginary part of the complex dielectric permittivity, μ_r'' the imaginary part of the complex permeability and $\mathbf{H}$ is the magnetic field.

The electromagnetic loss given by Equation (3) depends on both electric and magnetic fields. Assuming that the sample and the sample holder, who have low permeability numbers, are placed in a maximum of the electric stationary wave, the magnetic part of the heat source can be neglected [12–14], and Equation (3) can consequently be simplified as:

$$Q_{EM} = \frac{1}{2}\omega \varepsilon_0 \varepsilon_r'' \mathbf{E}^2 \tag{4}$$

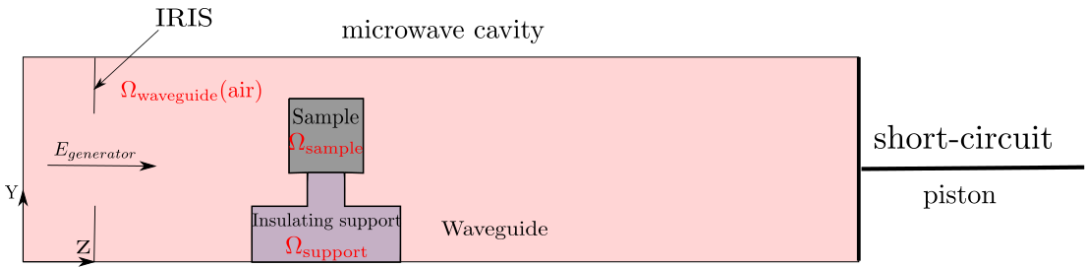

FIGURE 1 Single-mode microwave cavity with the SiC sample on an insulating support.

2.2 | Boundary conditions

The boundary conditions associated to the electromagnetic and thermal problems are sum up in Figure 2 . More precisely, to close the electromagnetic problem (1), a rectangular "port" condition, in the COMSOL Multiphysics® denomination [24], is considered. This condition consists in defining the power of the incident electric wave and its mode of propagation (transverse electromagnetic mode TE_{10p}). In addition, the cavity walls are considered as perfect electric conductors: the wave is totally reflected by the internal surface of the cavity, *i.e* $\mathbf{n} \times \mathbf{E} = \mathbf{0}$ on this surface, where $\mathbf{n}$ is the unit vector orthogonal to the cavity walls (see Figure 2 a). Concerning the thermal problem (2), a radiative flux Φ_r, evaluated with respect to the ambient temperature

$T_{amb} = 293$ K, and a convective flux Φ_c, are considered on the surface Γ_{r-c} of the sample (Figure 2 b). The normal component of these fluxes is given, respectively, by

$$\Phi_r = \sigma_B \epsilon (T^4 - T_{amb}^4) \tag{5}$$

and

$$\Phi_c = h\,(T - T_{amb}) \tag{6}$$

where σ_B is the Stefan-Boltzmann's constant, ϵ the emissivity, and h is the convection exchange coefficient ($h = 5$ W.m^{-2}.K^{-1} in our simulations). At the sample / support interface (denoted Γ_{cond} in Figure 2 b), the thermal conductivity considered is the average of the sample and insulating support conductivities. In addition, the external surface of the support is considered to be thermally insulated.

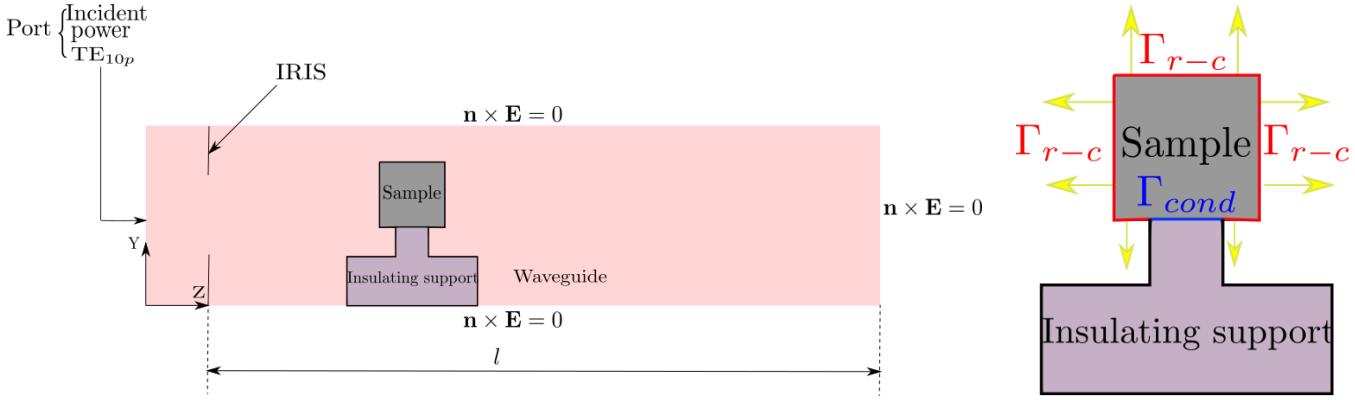

(a) Electromagnetic problem **(b)** Thermal problem

FIGURE 2 Boundary conditions.

2.3 | Waveguide dimensions

A rectangular waveguide of section $a \times b$, $a = 86.68$ mm and $b = 43.18$ mm (Figure 8), with an adjustable length l delimited by an iris and a short-circuit piston (Figures 4 a and 4 b), is used in this work. The iris has two roles: it allows the wave coming from the generator to enter the cavity, and it reflects all or part of the wave reflected by the short-circuit piston. The length of a perfect empty cavity can be deduced from the expression of the resonant frequency ω_{nmp} (corresponding to a stationary wave):

$$\omega_{nmp} = c\sqrt{\left(\frac{n\pi}{a}\right)^2 + \left(\frac{m\pi}{b}\right)^2 + \left(\frac{p\pi}{l}\right)^2} \tag{7}$$

where c is the speed of light in vacuum, n, m, p are the mode coefficients. In our case, $n = 1$, $m = 0$ and $p = 4$ (TE$_{104}$ excitation), while the angular frequency of the generated microwaves is $\omega_{104} = 2\pi \times 2.45$ rad.s^{-1}. The corresponding theoretical

length of the empty cavity is $l = 345.44$ mm. As will be seen below, cavity lengths provided by experiments or simulations differ from this theoretical value for at least three reasons. First, the real cavity is not a perfect conductor, second the real cavity includes additional elements such as a chimney or iris (Figure 4), and third, all elements inside the cavity disturb the resonance. Therefore, the length of the single-mode cavity must be tuned by adjusting the length of the waveguide from the short-circuit side (Figure 4 a) to an ensure efficient heating.

3 | EXPERIMENTAL PROCEDURE

3.1 | Pyrometer calibration

Due to the microwave-metal interaction, the use of thermocouples is not suitable for measuring the temperature of SiC sample inside cavity. For this reason, infrared pyrometers are usually used. However, they must be calibrated for the specific material under consideration. In this work, an infrared pyrometer (Fluke® Process Instruments[27], E3ML-F1-V-0-0) operating at wavelength $\lambda = 2.4\mu$m is used. Calibration of the pyrometer requires determination of the SiC apparent emissivity in its environment over a certain temperature range, here [373 K - 1173 K]. This determination is performed by focusing the pyrometer on the sample placed in a conventional furnace under blackbody conditions[28]. The temperature of the sample is measured using a type K thermocouple connected to a data acquisition center. At stabilized and constant temperature, emissivity of the pyrometer is tuned to fit temperature of the type K thermocouple

A 99% grade SiC (SCERAM Advanced Ceramics[29] supplier) sample is parallelepipedic with dimensions 15.7 mm × 6.3 mm × 19 mm. The latter is positioned on the bottom of a SiC hollow cylinder of height $L = 61.47$ mm and inner diameter $d_{int} = 10$ mm satisfying the criteria to be in blackbody condition ($L/d_{int} > 4$[28], see Figure 3 a). The focal length, defined in Figure 3 a, is taken as $d_{focal} = 500$ mm, which respects the condition that the spot size, equal to $d_{focal}/100$ is smaller than the internal diameter of the cylinder d_{int}.

Calibration of the pyrometer is performed using a cycle programmed with a heating rate of 5 K/min and a temperature stage of 30 min for every 100 K from T_{amb} to 1173 K. The apparent emissivity is evaluated at the end of each temperature stage. Its temperature dependence is represented in Figure 3 b. This apparent emissivity increases from 0.88 to 0.98 when the temperature ranges from 373 K to 1173 K. The result is consistent with the value of 0.9 used by Manière *et al.*[2,8].

3.2 | Microwave set-up

Figure 4 presents the experimental set-up used to study microwave heating of the SiC sample. The single-mode cavity is composed of a 2.45 GHz microwave generator (Sairem GMSP10, Solid State[30]), a WR340 waveguide, an iris, appertures with cylindrical chimneys and a short circuit piston. The SiC sample is placed on an alumina-silica insulating support (80 % Al_2O_3 -

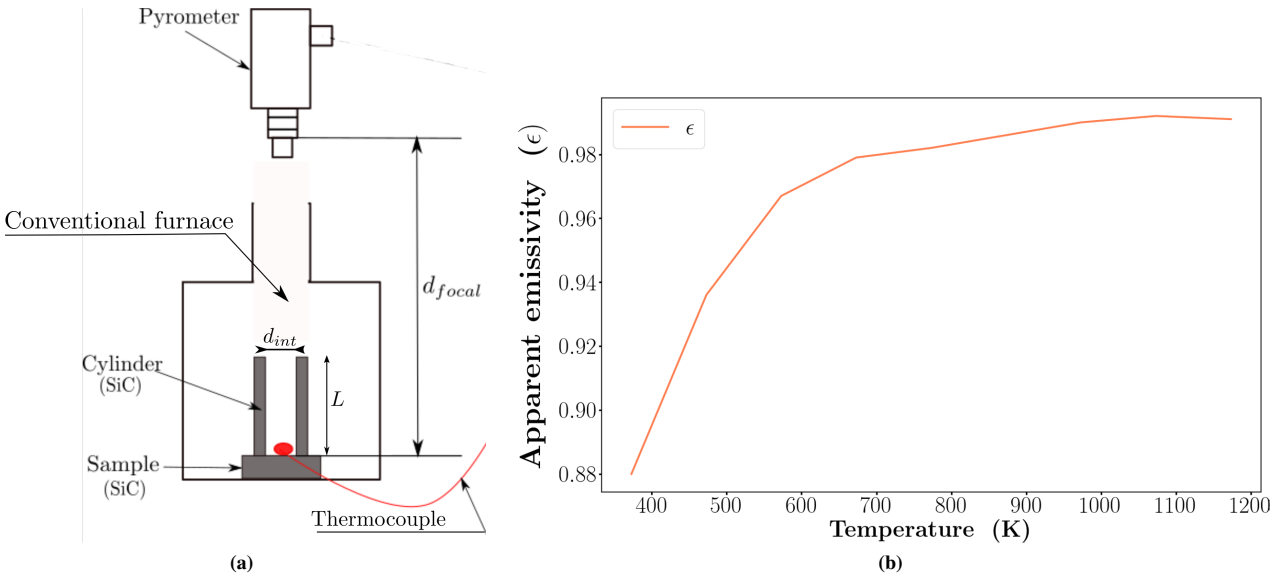

FIGURE 3 Pyrometer calibration: (a) material and method used, (b) emissivity evolution during heating cycle.

20% SiO_2), assumed to be transparent to microwaves. The geometry of the support was designed to minimize the surface area in contact with the SiC (Figure 4 a). In order to obtain an efficient heating of the sample, the heated system (sample and support) is placed in a maximum of the electric field. As discussed before, due to the dielectric parameters of the material, the electric field is disturbed and the cavity must therefore be tuned by changing the length l of the waveguide with the short circuit piston, until the reflected power P_r is minimized.

The heating is performed in considering four sample orientations. The figure 5 shows these orientations with respect to the electric field polarization $\vec{k}$. Each case corresponds to a different orientation of the sample in the cavity, and therefore with respect to the electric field.

For each sample orientation, the resonant length is first determined at room temperature in applying the nominal microwave power of 50 W and in monitoring the reflected power who vanishes at the resonance. The nominal microwave power of 50 W is then kept without subsequently changing cavity length during heating. For cases 1 to 4, the cavity length are 334.0 mm, 337.5 mm, 345.8 and 338.7 mm, respectively.

Time evolution of the reflected power P_r is presented in the Figure 6 . Once the resonance found, the reflected power increases until to reach a steady state which depends on the sample orientation. At steady state, the reflected power value ranges between 1 W (case 1) to 11 W (case 3).

Figure 7 presents the temperature change over time of the SiC sample for the four orientations. In each situation, the temperature increases until reaching a constant value after about 200 s. This steady temperature is 900 K, 860 K, 820 K and 820 K for case 1 to 4, respectively. The final temperature is correlated to reflected power as the lowest is the steady value of P_r, the highest is the steady temperature.

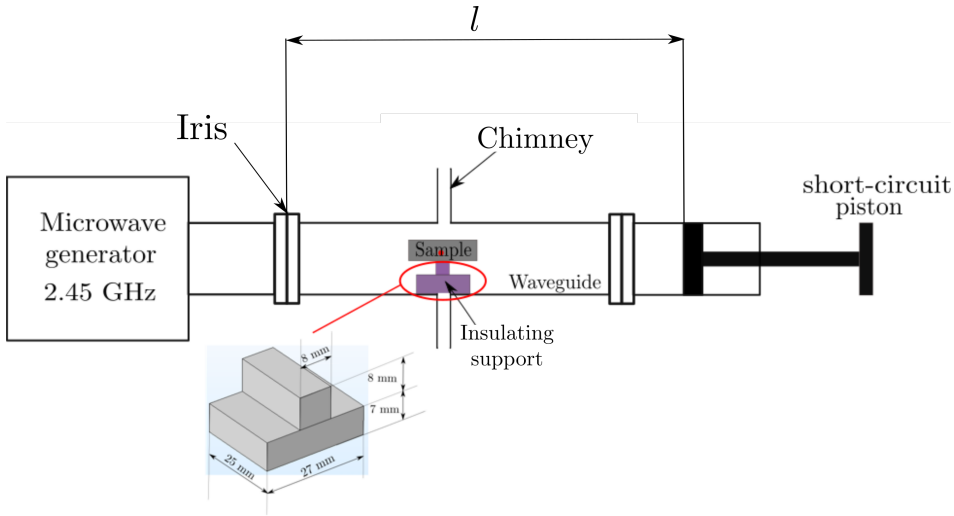

(a)

(b)

FIGURE 4 Schematics (a) and photography (b) of single-mode microwave device.

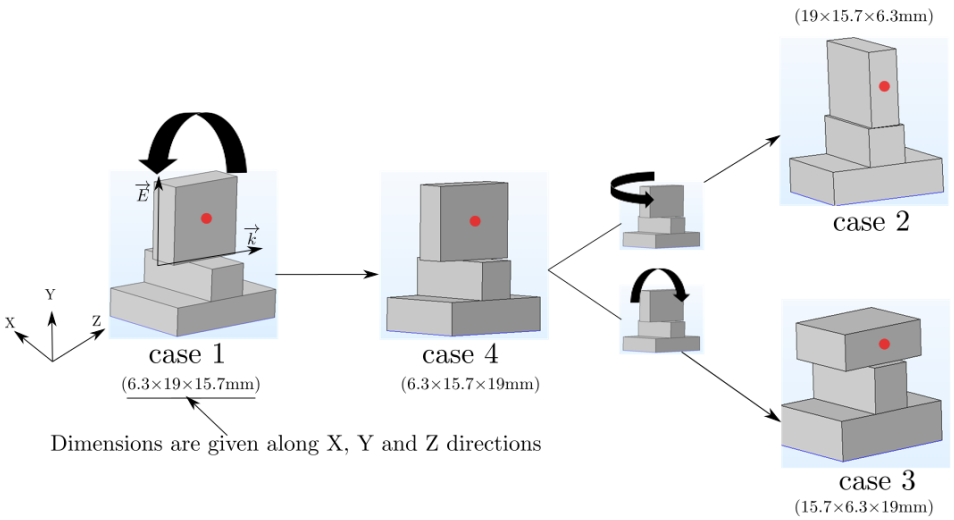

FIGURE 5 Different orientations studied for microwave heating. The red point is the point focused by the pyrometer.

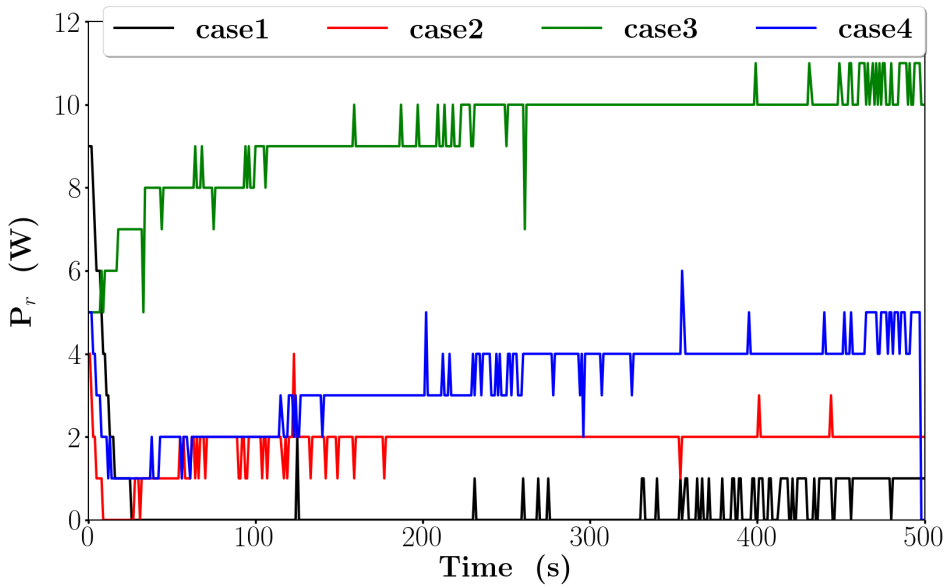

FIGURE 6 Reflected power for the four studied orientations, with an incident power $P_{in} = 50$ W.

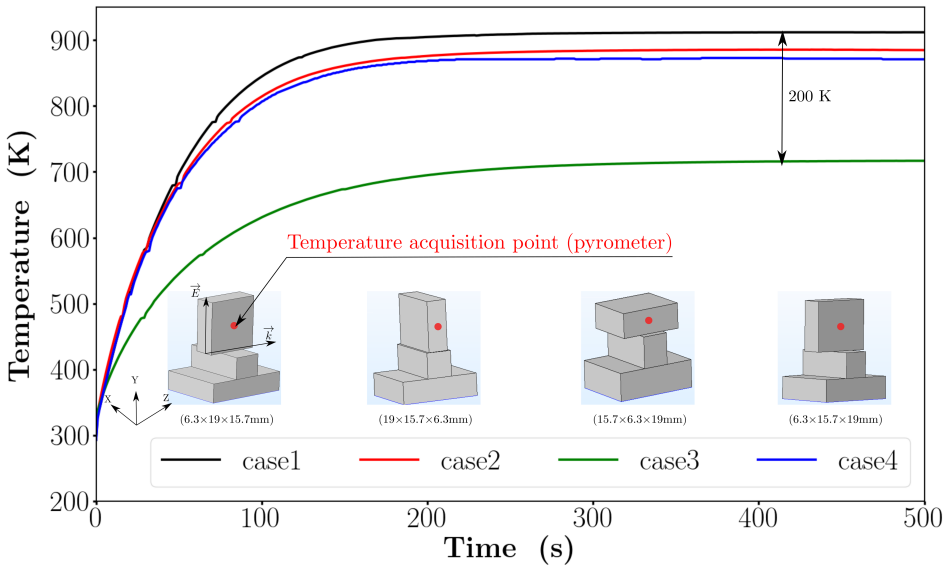

FIGURE 7 Temperature evolution during heating for the four configurations.

4 | NUMERICAL SET-UP

3D simulations of microwave heating are performed using the Finite Element (FE) software COMSOL Multiphysics®[24]. The electromagnetic problem (Equation (1)) is solved by a frequency approach, whereas the thermal problem (Equation (2)) is solved by using a FE approximation in space, combined with an implicit time discretisation. In this work, simplicial meshes and continuous piecewise linear approximations of both electric and temperature fields are considered. In comparison to experiment set-up (Figure 4 a), the geometry of the cavity considered in our simulations is simplified and is presented in Figure 8 . Indeed, the holes and cylindrical chimneys are not taken into account in order to reduce the computation cost.

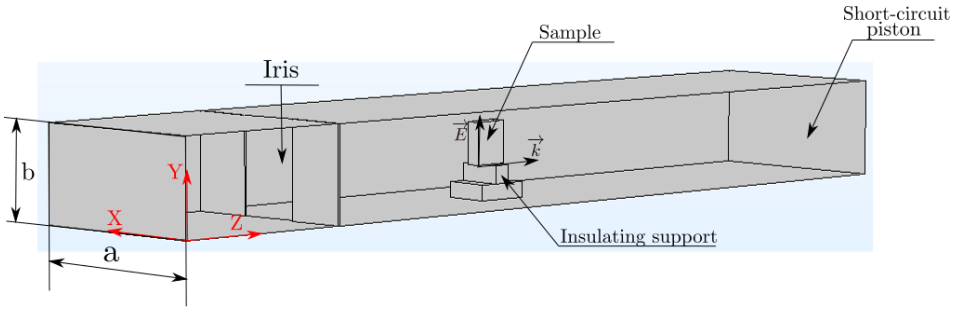

FIGURE 8 3D geometry of microwave cavity.

The boundary conditions are described in Section 2. The electromagnetic and thermal properties of the SiC sample and alumina-silicate support, are given in Appendix A1 as polynomial functions of temperature.

Regarding the high values of the SiC dielectric constant, the support is assumed to be transparent to microwave, *i.e.* $\epsilon_r' = 1$ and $\epsilon_r'' = 0$.

4.1 | Mesh sensitivity analysis

A sensitivity analysis of the temperature to the mesh is first conducted in order to evaluate which mesh size can be chosen to limit the computation time while having an acceptable discretisation error. Three different meshes, all made up of tetrahedrons, are considered: a coarse mesh, a fine mesh and a very fine mesh. The corresponding characteristic lengths of elements used for discretising cavity, sample and support are presented in Table 1 .

The mesh size sensibility is conducted on the case 1 (Figure 5) using a constant incident power $P_{in} = 50$ W. The temperature evolution obtained with the three meshes is plotted in Figure 9 . A difference of 60 K is found on the equilibrium temperature calculated with the coarse and fine meshes, whereas no significant difference appears when fine and very fine meshes are used. Table 2 presents the computational time with respect of the number of degrees of freedom (DOF) of the coupled problem,

TABLE 1 Characteristic lengths of elements of cavity, sample and insulating support for coarse, fine and very fine meshes.

Characteristic lengths (mm)	Coarse mesh	Fine mesh	Very fine mesh
Cavity	[7.6 - 42.3]	[4 - 7]	[2 - 3.5]
Sample & support	[8.45×10^{-2} - 8.4]	2	[0.1 - 1]

obtained after 500 time increments. The computational time increases by a factor of ten when switching from the fine mesh to the very fine mesh, while the quality of the results does not seem to be improved accordingly. Therefore, the fine mesh is retained in the simulations presented in the next section.

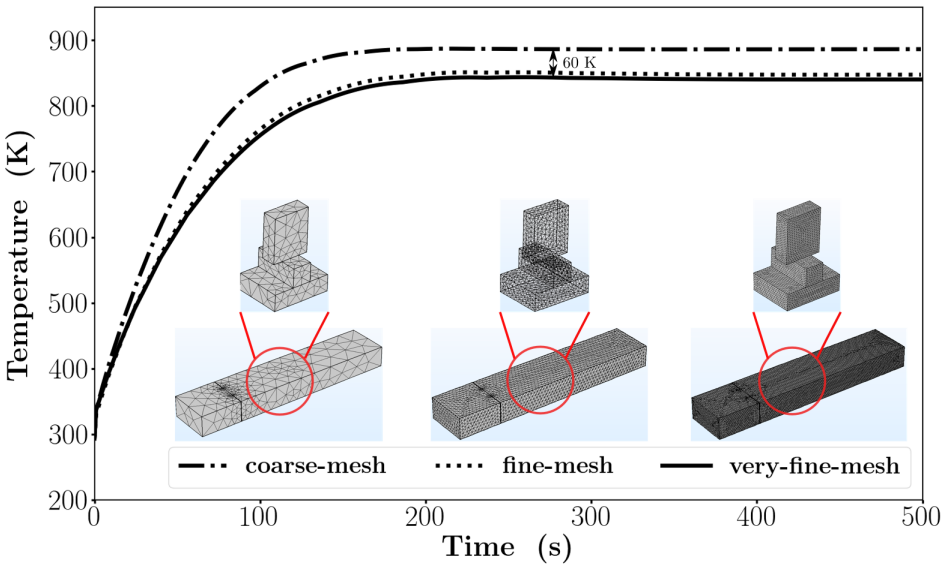

FIGURE 9 Mesh sensitivity analysis: temperature evolution for three different meshes.

TABLE 2 Mesh sensitivity analysis: number of DOF and computation time (on 12 cores of an Intel Xeon Gold 6128 bi-processor at 3.4 GHz) for three different meshes.

	Coarse mesh	Fine mesh	Very fine mesh
DOF	4.3×10^4	6.7×10^5	5.1×10^6
Computation time (s)	1.3×10^2	1.5×10^3	1.3×10^4

4.2 | Numerical results

Before simulating the microwave heating, the resonance of the cavity has to be set by adjusting the length of waveguide. This setting allows the existence of a stationary wave: the incident and reflected waves are in phase, their maxima add therefore together, and a constructive interference occurs. At room temperature, the length obtained for the existence of a TE_{104} mode in the empty cavity is 342 mm. This value differs from the theoretical value of 345.44 mm given by relation (7), due to certain differences in geometry (presence of an iris in the simulations). Figure 10 a shows the intensity of the computed electric field in such an empty cavity, represented in the YZ plan. As expected, the electric field has four maxima since a TE_{104} excitation has been prescribed. The maximal intensity in this case is 6.49×10^4 V/m.

When the sample and the support are inserted in the cavity, the electric field is modified. Figure 10 b presents the new electric field for the orientation corresponding to case 1. The incident and reflected waves are no longer in phase: four maxima are still detected but with lower intensity, equal to 1.39×10^4 V/m. The resonance is recovered by adjusting the length of the waveguide with the criterion of maximizing the electric field intensity, or alternatively, minimizing the reflected power P_r. Thus, the resonance is reached for a cavity of 336.5 mm. The corresponding electric field is represented in Figure 10 c, with a maximum equal to 9.31×10^4 V/m. It can be seen that the highest magnitude is not within the sample, but outside it. This is due to the high value of the real part of the SiC permittivity (see Appendix A) compared to that of the air in Ω_{cavity} ($\varepsilon_r = 1$)[20].

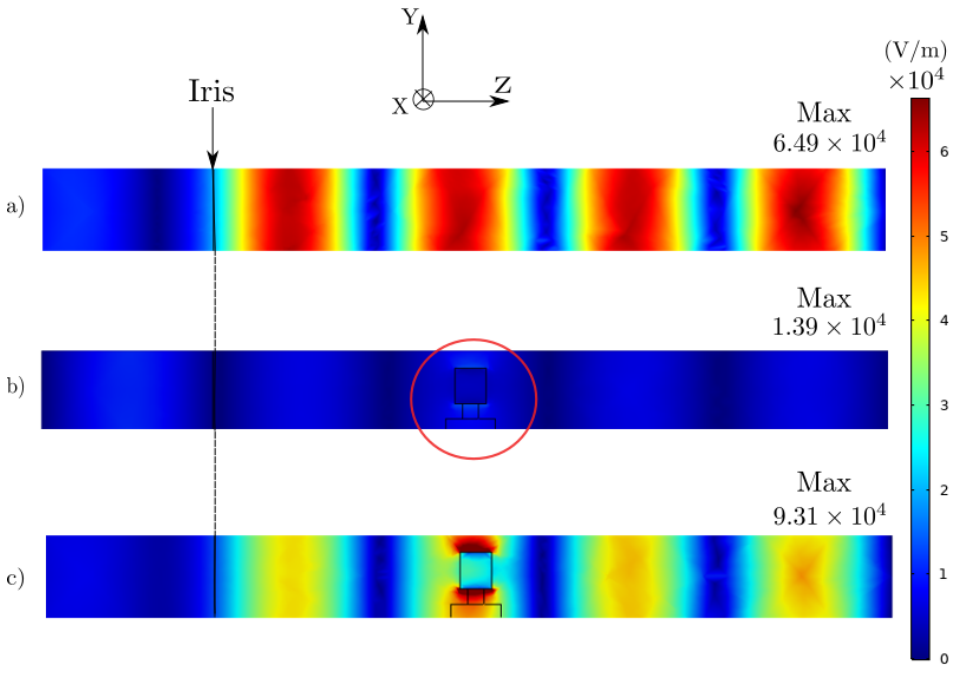

FIGURE 10 Computed electric field a) empty cavity, b) cavity, sample and insulating support before resonance, c) cavity, sample and insulating support at resonance for case 1.

For each orientation, the cavity length is set at room temperature, where the average of the electric field intensity over the whole domain is maximum at the resonance. These average values are plotted with respect to the cavity length in Figure 11 for the four orientations. Additionally, the lengths determined experimentally are represented in this figure by star markers. The difference between the lengths measured experimentally and the simulated lengths, varies from 0.36 mm for case 2, to 6.3 mm for case 3. This difference comes from the assumptions made in the simulations: simplified geometry, cavity walls considered to be perfectly electrically conductive, insulating support transparent to microwaves.

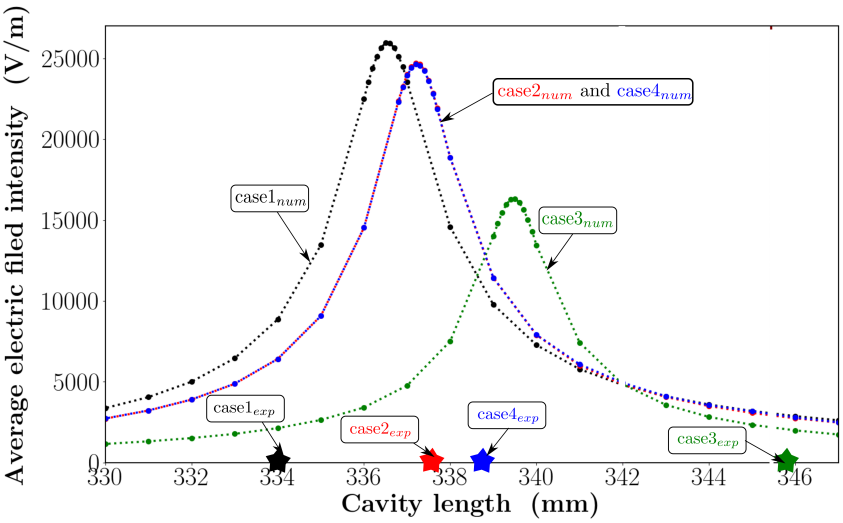

FIGURE 11 Average intensity of the electric field obtained by simulation for different cavity lengths, in the four investigated cases. Star markers correspond to the resonant lengths measured experimentally.

Using a constant power of 50 W, the microwave heating of the SiC sample is now investigated. The experimental and numerical temperatures, measured at the sample surface, are plotted as functions of time in Figure 12 , for the four cases studied. A good agreement between the simulation and the experimental results is observed for all four cases. Despite slightly lower kinetics to reach equilibrium in the numerical description, the temperature difference at steady state is 2 K for case 1 and in the order of 20 K for the other cases. These results indicate that the approximations done are not so restrictive to reproduce the experimental results (insulating support considered as transparent to microwaves, cavity walls considered to be a perfect conductor, no description of the chimney) and that the material parameters used are reliable. As expected, the orientation of the sample has a huge impact on the heating. The maximum temperature at steady state is obtained for case 1 (T=916.5 K), followed by case 2 (T=905 K), case 4 (T=892 K) and case 3 (T=735 K), respectively (Figure 12). This result is related to the polarization field which is higher when the sample is oriented along the electric field. In such situations, the dipolar losses are higher leading to a better heating, as more energy is absorbed and converted into heat. The simulations nicely recover this effect since the correspondence between

the equilibrium temperature and the height of the sample in the direction of the electric field direction is respected. Note that the equilibrium temperature is correlated with the maximum values of average electric field intensity presented in Figure 11 . The slight different between case 2 and case 4 may result from the difference of the surface area in contact between the sample and the insulating support.

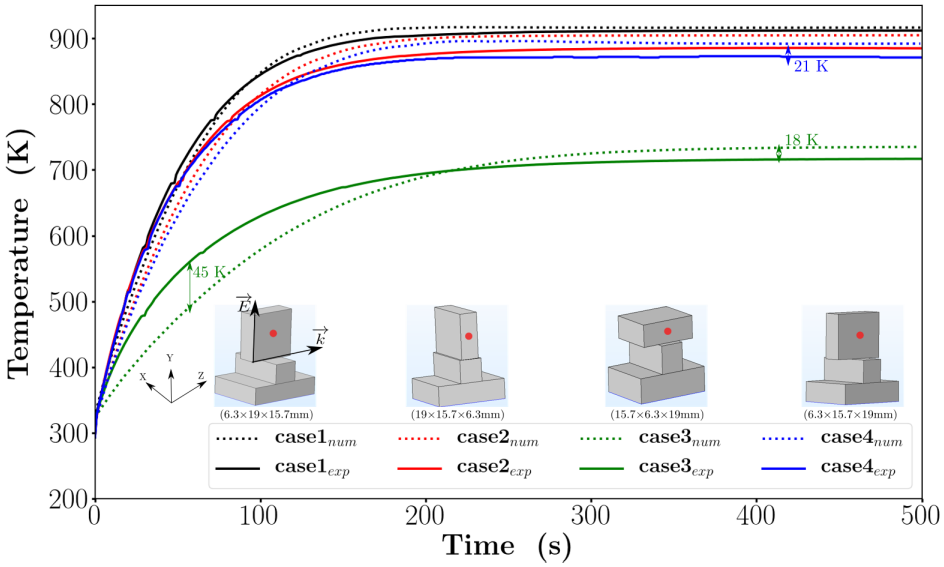

FIGURE 12 Evolution of experimental and numerical temperatures during microwave heating, for the four sample orientations investigated.

As mentioned previously, the heating is very sensitive to the length of the waveguide, which must be adjusted to maximize the stationarity of the waves. Figure 13 presents the equilibrium temperature at the sample surface as a function of the length of the waveguide, for the different sample orientations. These curves show that the length of the cavity has to be set with accuracy to produce optimal heating of the sample. A deviation of one millimeter from the resonance length can lead to a drastic drop in the equilibrium temperature. In the simulations, a precision of one tenth of a millimeter on the length of the cavity is required to optimize the heating. It can be noted that the resonance length also correlates with the orientation of the sample with the same trend obtained for the equilibrium temperature. Thus, the shortest cavity length corresponds to case 1 where the highest dimension of the sample is aligned with the electric field.

5 | CONCLUSIONS

The purpose of this paper was to study the microwave heating of a parallelepipedic sample in silicon carbide, a material with a high dielectric loss at room temperature. This study was carried out both experimentally and numerically at the macroscopic

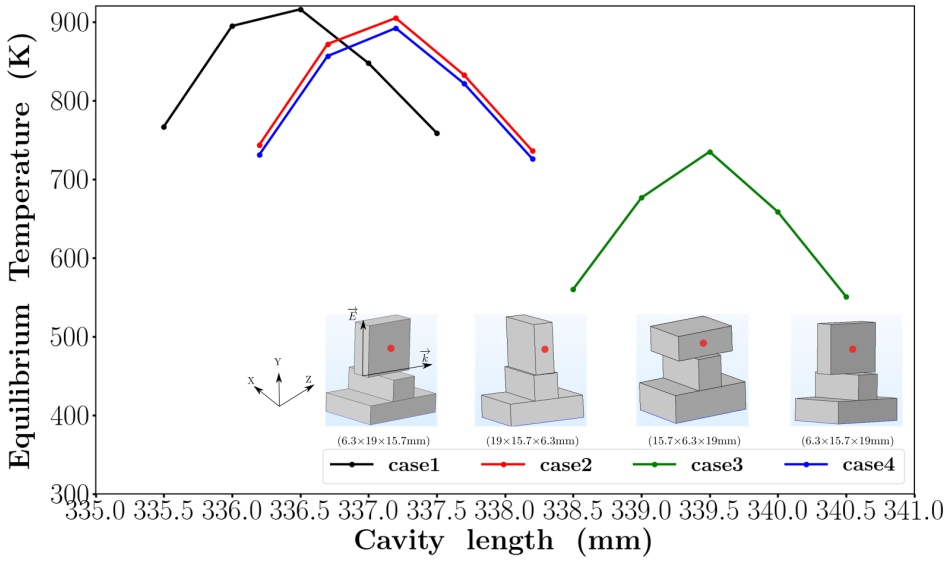

FIGURE 13 Equilibrium temperature as a function of the cavity length for the different sample orientations.

scale. The experimental procedure first requires calibration of the pyrometer in a conventional furnace where the use of a thermocouple is appropriate. Apparent SiC emissivity is measured in this environment. The sample is then placed in a 2.45 GHz single-mode cavity. Four different orientations are considered. After adjusting the length of the cavity to the resonant length at room temperature, the sample is heated with a constant power of 50W. The numerical simulations, performed using the finite element software COMSOL Multiphysics® , consisted in solving an electromagnetic - thermal problem under the same conditions as in the experimental procedure. Despite the approximations made in the numerical modelling (insulating support considered transparent to microwaves, cavity wall considered to be a perfect conductor, no description of the chimney), a good agreement between the simulations and the experimental results is found for all four cases. In particular, the most efficient heating is obtained when the sample is oriented along the electric field. The sensitivity of the electric field, and thus of the heating, to the length of the cavity was also highlighted.

Even if the numerical model can always be improved (*e.g.* by using measured values of the dielectric loss of the insulating support), these results show that we can be confident in the ability of the simulations to capture accurately the behaviours shown in the experimental results. Such simulations could provide relevant data for analyzing the bulk temperature of complex-shaped parts. Additionally, in future work, this model will contribute to simulate the heating and sintering of an alumina sample in a hybrid configuration, *i.e.* with SiC susceptors. In this context, challenges are to characterize the densification and the evolution of material properties during sintering. It involves to link microstructures and material properties. A fine description of temperature gradients in the sample would allow to understand the densification gradients as well as the sample distortion that may appear.

Finally, such a numerical model makes it possible to predict the final shape, and to optimize the position of susceptors and the sample in the cavity.

References

1. Rybakov KI, Olevsky EA, and Krikun EV. Microwave Sintering: Fundamentals and Modeling. J Am Ceram Soc. 2013 March;**96**:1003–1020.

2. Manière C, Geuntak L, Zahrah T, and Olevsky EA. Microwave flash sintering of metal powders: From experimental evidence to multiphysics simulation. Acta Mater. 2018;**147**:24–34.

3. Agrawal D. Microwave sintering of metal powders. In: Chang I, and Zhao Y, editors. Advances in Powder Metallurgy. Woodhead Publishing; 2013. p. 361–379.

4. Roy R, Agrawal DK, Cheng J, and Gedevanishvili S. Full sintering of powdered-metal bodies in a microwave field. Nature. 1999;**399**:668–670.

5. Karayannis V. Microwave sintering of ceramic materials. IOP Conf Ser: Mater Sci Eng. 2016 12;**161**:012068.

6. Manière C, Chan S, and Olevsky EA. Microwave sintering of complex shapes: From multiphysics simulation to improvements of process scalability. J Am Ceram Soc. 2019;**102**(2):611–620.

7. Marinel S, Manière C, Bilot A, Bilot C, Harnois C, Riquet G, et al. Microwave Sintering of Alumina at 915 MHz: Modeling, Process Control, and Microstructure Distribution. Materials. 2019 08;**12**:2544.

8. Manière C, Zahrah T, and Olevsky EA. Fully coupled electro-magnetic-thermal-mechanical comparative simulation of direct vs hybrid microwave sintering of 3Y-ZrO2. J Am Ceram Soc. 2016;**100**(6):2439–2450.

9. Croquesel J, Bouvard D, Chaix JM, Carry CP, and Saunier S. Development of an instrumented and automated single mode cavity for ceramic microwave sintering: Application to an alpha pure alumina powder. Mater Design. 2015;**88**:98–105.

10. Mishra RR, and Sharma AK. Microwave-material interaction phenomena: Heating mechanisms, challenges and opportunities in material processing. Compos Part A-Appl S. 2016;**81**:78–97.

11. Makino Y, Ohmae T, Setsuhara Y, Miyake S, and Sano S. Sintering of Al2O3-ZrO2 Composites Using Millimeter-Wave Radiation. In: The Science of Engineering Ceramics II. vol. 161 of Key Engineering Materials. Trans Tech Publications Ltd; 1998. p. 41–44.

12. Shi J. Experiment and simulation of micro injection molding and microwave sintering. Université de Franche-Comté; 2014.

13. Saltiel C, and Datta AK. Heat and Mass Transfer in Microwave Processing. In: Hartnett JP, Irvine TF, Cho YI, and Greene GA, editors. Adv Heat Transfer. vol. 33. Elsevier; 1999. p. 1–94.

14. Manière C, Zahrah T, and Olevsky EA. Inherent heating instability of direct microwave sintering process: Sample analysis for porous 3Y-ZrO2. Scr Mater. 2017;**128**:49–52.

15. Olevsky EA, and Dudina DV. Field-assisted Sintering: Science and Applications. New York, NY: Springer International Publishing AG; 2018.

16. Pert E, Carmel Y, Birnboim A, Olorunyolemi T, Gershon D, Calame J, et al. Temperature Measurements during Microwave Processing: The Significance of Thermocouple Effects. J Am Ceram Soc. 2001;**84**(9):1981–1986.

17. Olevsky EA. Theory of sintering: from discrete to continuum. Mater Sci Eng, R. 1998;**23**(2):41–100.

18. Charmond S, Carry CP, and Bouvard D. Densification and microstructure evolution of Y-Tetragonal Zirconia Polycrystal powder during direct and hybrid microwave sintering in a single-mode cavity. J Eur Ceram Soc. 2010;**30**(6):1211–1221.

19. Zuo F, Saunier S, Marinel S, Chanin-Lambert P, Peillon N, and Goeuriot D. Investigation of the mechanism(s) controlling microwave sintering of α-alumina: Influence of the powder parameters on the grain growth, thermodynamics and densification kinetics. J Eur Ceram Soc. 2015;**35**(3):959–970.

20. Heuguet R, Marinel S, Thuault A, and Badev A. Effects of the Susceptor Dielectric Properties on the Microwave Sintering of Alumina. J Am Ceram Soc. 2013 08;**96**:3728–3736.

21. Iskander MF, Smith RL, Andrade AOM, Kimrey H, and Wal LM. FDTD simulation of microwave sintering of ceramics in multimode cavities. IEEE Trans Microwave Theory Tech. 1994 May;**42**(5):793–800.

22. White MJ, Iskander MF, and Huang Z. Development of a multigrid FDTD code for three-dimensional applications. IEEE Trans Antennas Propag. 1997 Oct;**45**(10):1512–1517.

23. White MJ, Iskander MF, Huang Z, and Kimrey HD. A three dimensional multi-grid FDTD code for modeling microwave sintering of materials. In: IEEE Antennas and Propagation Society International Symposium. 1996 Digest. vol. 1; 1996. p. 120–123.

24. COMSOL Multiphysics®. Url=https://www.comsol.com;.

25. Regier M, Knoerzer K, and Schubert H. 1 - Introducing microwave-assisted processing of food: Fundamentals of the technology. In: Regier M, Knoerzer K, and Schubert H, editors. The Microwave Processing of Foods (Second Edition).

second edition ed. Woodhead Publishing Series in Food Science, Technology and Nutrition. Woodhead Publishing; 2017. p. 1–22.

26. Guenther BD. Electromagnetic Theory. In: Modern Optics. 2nd ed. Oxford ; New York, NY: OUP Oxford; 2015. p. 15–51.

27. Fluke® Endurance® Series documentation. Url=http://support.fluke.com/ircon-sales/Download/Asset/6006198_6252_ENG_E_W.PDF;.

28. Sparrow E, Albers L, and Eckert E. Thermal radiation characteristics of cylindrical enclosures. J Heat Transfer. 1962;**84**(1):73–79.

29. SCERAM Advanced Ceramics. Url=https://www.sceram.com/carbure-de-silicium/;.

30. SAIREM documentation. Url=https://www.sairem.com/wp-content/uploads/2019/02/GMSP10-EN.pdf;.

31. Baeraky TA. Microwave measurements of the dielectric properties of silicon carbide at high temperature. Egypt J Sol. 2002;**25**(2):263–273.

32. MatWeb Material Property Data. Url=http://www.matweb.com/;.

APPENDIX

A ELECTROMAGNETIC-THERMAL MATERIAL PROPERTIES

TABLE A1 Electromagnetic-thermal material properties.

Material	Symbol (unit)	Temperature range (K)	Expression
Insulation [8]	C_p (J.kg^{-1}.K^{-1})	273-1200 K	$5.82\times10^{2}+1.25T-5.31\times10^{-4}T^{2}$
	κ (W.m^{-1}.K^{-1})	273-1200 K	$6.15\times10^{-2}+1.74\times10^{-4}T$
	$\overline{\rho}$ (kg.m^{-3})	273-1200 K	$4.43\times10^{2}-1.04\times10^{-2}T$
	ϵ	273-1200 K	0.83
	ε_r	273-1200 K	1. (microwave transparent)
SiC [31, 32]	C_p (J.kg^{-1}.K^{-1})	273-673 K	$-8.35+3.08T-0.00293T^{2}+1.0268\times10^{-6}T^{3}$
		673-1200 K	$772+0.431T-2.1\times10^{-5}T^{2}$
	κ (W.m^{-1}.K^{-1})	273-1200 K	$192-0.326T+2.74\times10^{-4}T^{2}-7.71\times10^{-8}T^{3}$
	$\overline{\rho}$ (kg.m^{-3})	273-1200 K	$2977+0.051T-2.29\times10^{-4}T^{2}+2.98\times10^{-7}T^{3}$ $-1.92\times10^{-10}T^{4}+4.77\times10^{-14}T^{5}$
	ϵ	273-1200 K	$-1.239\times10^{-12}T^{4}+4.51\times10^{-9}T^{3}-6.1142\times10^{-6}T^{2}$ $+0.0037T+0.1436$
	$\varepsilon_r^{'}$	273-1200 K	$6.4-1.67\times10^{-3}T+1.88\times10^{-6}T^{2}$
	$\varepsilon_r^{\varepsilon}$	273-1200 K	$0.992-3.43\times10^{-4}T+7.72\times10^{-6}T^{2}-7.15\times10^{-9}T^{3}$ $+2.36\times10^{-12}T^{4}$
Air [7]	C_p (J.kg^{-1}.K^{-1})	273-1200 K	$961+0.177T$
	κ (W.m^{-1}.K^{-1})	273-1200 K	$0.0035+6\times10^{-5}T$
	$\overline{\rho}$ (kg.m^{-3})	273-1200 K	0.02897P/(RT)
	ε_r	273-1200 K	1